Jamming, hysteresis, and oscillation in scalar models for shear thickening

D. A. Head,[1] A. Ajdari,[2] and M. E. Cates[1]

[1]*Department of Physics and Astronomy, JCMB King's Buildings, University of Edinburgh, Edinburgh EH9 3JZ, United Kingdom*
[2]*Laboratoire de Physico–Chimie Théorique, Esa CNRS 7083, ESPCI, 10 rue Vauquelin, F-75231 Paris Cedex 05, France*

We investigate shear thickening and jamming within the framework of a family of spatially homogeneous, scalar rheological models. These are based on the "soft glassy rheology" model of Sollich *et al.* [Phys. Rev. Lett. **78**, 2020 (1997)], but with an effective temperature x that is a decreasing function of either the global stress σ or the local strain l. For appropriate $x=x(\sigma)$, it is shown that the flow curves include a region of negative slope, around which the stress exhibits hysteresis under a cyclically varying imposed strain rate $\dot{\gamma}$. A subclass of these $x(\sigma)$ have flow curves that touch the $\dot{\gamma}=0$ axis for a finite range of stresses; imposing a stress from this range *jams* the system, in the sense that the strain γ creeps only logarithmically with time t, $\gamma(t) \sim \ln t$. These same systems may produce a finite asymptotic yield stress under an imposed strain, in a manner that depends on the entire stress history of the sample, a phenomenon we refer to as *history-dependent jamming*. In contrast, when $x=x(l)$ the flow curves are always monotonic, but we show that some $x(l)$ generate an oscillatory strain response for a range of steady imposed stresses. Similar spontaneous oscillations are observed in a simplified model with fewer degrees of freedom. We discuss this result in relation to the temporal instabilities observed in rheological experiments and stick-slip behavior found in other contexts, and comment on the possible relationship with "delay differential equations" that are known to produce oscillations and chaos.

I. INTRODUCTION

A wide variety of materials can be driven into a non-equilibrium state that is either solidlike and static, or fluid-like but only relaxes on time scales that far exceed the experimental time frame, if at all. Such states are often referred to as "jammed," and are realizable in molecular liquids having undergone a rapid quench to low temperatures, or colloids at a high volume fraction, to cite just two examples [1,2]. It has recently been postulated by Liu and Nagel that the nature of the jammed state may be independent of the manner in which it was formed [3]. For example, a stress-induced jamming transition may produce a qualitatively similar state to a temperature-induced transition. This was expressed in the form of a "jamming phase diagram," in which jammed configurations occupy a compact region near to the origin of a phase space comprised of three axes: the temperature T, the volume V, and the load σ [3,4].

In its simplest form, the Liu-Nagel jamming phase diagram suggests that increasing the applied load can only increase the likelihood of flow. However, it is equally feasible for an applied load to induce a jammed state. For instance, if a pile of sand is formed and then gravity is switched off, the system unjams without any significant variation in volume. Thus the load (here controlled by gravity) jams the system. This concurs with the earlier claim that jammed systems may be classified as "fragile"—that is, they can support only certain, *compatible* loads, and will rearrange or flow under an incompatible load [5]. Furthermore, one could also envisage a class of loadings that can alternately induce and destroy a jammed state as the magnitude of the load increases, a situation that could be referred to as "reentrant jamming."

The purpose of this paper is to investigate the nature of

transitions to or from jammed configurations that have, as their control parameter, the imposed shear stress σ. We do this by providing concrete examples of models that exhibit jamming transitions with σ, including instances of the reentrant jamming scenario described above. These models are based on the "soft glassy rheology" (SGR) model of Sollich *et al.* [6–8], which was originally devised to highlight the possible existence of glassy relaxation in a range of soft materials, such as foams, emulsions, pastes, etc. It is parametrized by an effective temperature x, which in the context of soft matter is thought to represent some form of mechanical noise, but may refer to the true thermal temperature in other applications.

As it was originally defined, the SGR model only exhibits shear thinning, which is clearly unsuitable for our purposes. Therefore, we consider variants of the model in which the effective temperature x is no longer constant, but can vary with the state of the system. More precisely, x is treated a function of both the global stress σ and the local strain l, i.e., $x=x(\sigma,l)$. By choosing suitable forms of $x(\sigma,l)$, systems can be constructed that become "colder" as they become more stressed, which allows for the system to shear thicken and even "jam."

For clarity, we restrict our attention to two limiting forms of $x(\sigma,l)$, namely, $x(\sigma)$ and $x(l)$. In the former case, certain classes of $x(\sigma)$ are shown to exhibit a flow curve (i.e., the curve of the stress σ versus the strain rate $\dot{\gamma}$ under conditions of steady flow) that is nonmonotonic, and can touch the $\dot{\gamma}=0$ axis for range of finite values of σ. Thus a "jammed" state with $\dot{\gamma}=0^+$ can be reached for some σ but not for others. Furthermore, it is also shown that, for systems driven by an imposed $\gamma(t)$, whether or not a jammed configuration is approached at late times depends on the entire strain his-

tory of the system, and not just the behavior of $\gamma(t)$ as $t \rightarrow \infty$. We refer to this phenomenon as "history-dependent jamming."

The behavior of systems with $x = x(l)$ is somewhat different, but no less remarkable. When driven by an imposed σ, certain forms of $x(l)$ exhibit a regime in which the viscosity never reaches its steady flow value but oscillates in time, with a wave form that is approximately sinusoidal near to the transition point, but becomes increasingly sharp deep into the oscillatory regime. The models considered here are spatially homogeneous, and so this oscillation is purely temporal, having no spatial component. It is tempting to associate these oscillations with the stick-slip behavior observed in granular systems and plate tectonics [9–12], but we shall give reasons why we believe that the underlying physics might be rather different. We cannot rule out the possibility of more complex oscillatory behavior, maybe even chaotic, arising in as-of-yet unobserved regions of parameter space.

The finding of a bifurcation to oscillatory behavior for $x = x(l)$ is all the more remarkable because the flow curve (as already defined) is everywhere monotonic increasing for this class of x. By contrast, instances of rheological instabilities that have been found experimentally have tended to occur for ranges of parameters in which the flow curve has a negative gradient [13–19]. This suggests that mechanism behind the instability observed here may be qualitatively different to those cited above, and may be realizable in some range of materials that has yet to be identified.

This paper is arranged as follows. In Sec. II the class of models to be studied is defined, with particular attention being paid to those aspects that differ from the SGR model. The known results of the SGR model that are relevant to the subsequent discussion are then briefly summarized in Sec. III. Systems with $x = x(\sigma)$ are described in Sec. IV, where it explained how the flow curves can be graphically interpreted as mappings from the SGR flow curves. The time-dependent behavior of the system has been found by numerical integration of the governing master equation. An example of history-dependent jamming is presented, and explained in terms of the stability of the steady flow solutions.

In Sec. V we turn to consider the case $x = x(l)$, and analytically prove that the flow curve is everywhere monotonic. Nonetheless, the simulations results presented here clearly show that $\dot{\gamma}(t)$ can oscillate in time for a range of imposed stresses σ. A qualitative explanation of the emergence of the oscillatory phase is also given, in terms of the model's internal degrees of freedom. The intensive nature of the simulations has meant that only a small range of functional forms for $x(l)$ have been investigated, and hence it has not been possible to fully characterize this range of models. Therefore, we consider a simplified model in Sec. VI, for which the simulation times are significantly shorter and a more complete picture has been realized. Some results of this model have also been presented elsewhere [20]. This reduced model clearly shows that the mean value of $\dot{\gamma}$ during the oscillatory motion deviates from the steady flow value by as much as an order of magnitude. Finally, in Sec. VII we discuss some

outstanding issues raised by this work, before summarizing our results in Sec. VIII.

II. MODELS OF THE SGR TYPE

All of the models studied in this paper represent generalizations of the SGR model of Sollich *et al.* [6–8]. It is, therefore, prudent, to first describe those features that are common to this class of models, before considering each of the different generalizations in turn. This is the purpose of the current section. Since the various assumptions that lie behind the construction of the SGR model have already been discussed at length elsewhere, we shall here give just a brief overview of the derivation and refer the reader to Refs. [6–8] for more detailed physical arguments. Only those aspects that differ from the SGR model will be discussed in full.

Our goal is to construct deliberately simplified models that exhibit shear thickening and jamming, but whose interpretation is more transparent than that of a detailed microscopic model. In this spirit, the models in this class all share a number of simplifications. Only single shear components of the strain and stress tensors are considered, which will be denoted by γ and σ, respectively. This is, therefore, a class of *scalar* models.

It is further assumed that the system can be coarse grained into a collection of mesoscopic subsystems, each of which are fully described by two scalar variables, namely, a local strain l and a stability parameter E. These mesoscopic subsystems will be referred to as *elements*. We simply assume here that such a coarse graining is possible, notwithstanding the significant practical challenges in constructing a suitable scheme for any given microscopic model.

At any given instant, each element has a probability of yielding per unit time that is denoted by $\Gamma = \Gamma(E, l)$. When an element yields, it is assumed that its microscopic constituents are rearranged to such a degree that it loses all memory of its former configuration. Its strain returns to zero, and it is assigned a new value of E that is drawn from a *prior* distribution $\rho(E)$. Suitable functional forms for $\Gamma(E, l)$ and $\rho(E)$ will be discussed below. The value of E remains fixed until the element yields again, but l follows the global strain γ according to $\dot{l} = \dot{\gamma}$. Thus the elements are affinely deformed by the flow field, which is assumed to be homogeneous.

Let us define $P(E, l, t)$ to be the probability density function of elements that have a local strain l and a barrier E at time t. Then $P(E, l, t)$ evolves in time according to two distinct mechanisms: the homogeneous shearing at a rate $\dot{\gamma}$, and the yielding of elements at a rate of $\Gamma(E, l)$ per unit time. Thus the master equation for $P(E, l, t)$ is

$$\frac{\partial}{\partial t} P(E, l, t) + \dot{\gamma} \frac{\partial}{\partial l} P(E, l, t) = -\Gamma(E, l) P(E, l, t)$$

$$+ \omega(t) \delta(l) \rho(E). \quad (1)$$

The second term on the left-hand side represents the increase in local strains l according to the uniform global strain rate $\dot{\gamma}$. The right-hand side describes the yielding of elements. The first term, which is negative, accounts for the loss

of elements as they yield at a rate $\Gamma(E,l)$. Conversely, the second term represents these same elements *after* they have yielded, which have a strain $l=0$ and a value of E drawn from $\rho(E)$. The total rate of yielding $\omega(t)$ is defined by

$$\omega(t) = \int_0^\infty dE \int_{-\infty}^\infty dl \, \Gamma(E,l) P(E,l,t) \qquad (2)$$

$$= \langle \Gamma(E,l) \rangle. \qquad (3)$$

Here we have introduced the notation that the angular brackets "$\langle \ldots \rangle$" represents the instantaneous average of the given function over $P(E,l,t)$. This will be used frequently in what follows.

The master equation (1) only describes the evolution of the strain degrees of freedom. To characterize the rheological response of the system, some relation must be found between the local strains l and the global stress σ. This involves two further assumptions. First, the elements are supposed to behave elastically between yield events, so that the local stress is just kl, where $k>0$ is a uniform elastic constant. Second, σ is the arithmetic mean of the local stresses, or $\sigma = \langle kl \rangle = k\langle l \rangle$. Other averaging procedures could be employed [21], but we focus here on the simplest nontrivial option. Although the local stress-strain relationship is elastic, the global stress also incorporates the yielding of elements and, as will be seen below, the σ-γ relationship is not a linear one.

We have been unable to find an analytic solution to the master equation (1) for any nontrivial $\Gamma(E,l)$. Instead it has been numerically integrated using the procedure summarized in Appendix A. However, it will sometimes be necessary to refer to the steady state solution for a constant $\dot{\gamma} \neq 0$, which can be found exactly,

$$P_\infty(E,l) = \frac{\omega_\infty}{\dot{\gamma}} \rho(E) \exp\left[-\frac{1}{\dot{\gamma}} \int_0^l dl' \Gamma(E,l') \right]. \qquad (4)$$

This is derived by setting $\partial_t P = 0$ in Eq. (1) and integrating the resulting first-order ordinary differential equation with respect to l. The asymptotic yield rate $\omega_\infty \equiv \lim_{t \to \infty} \omega(t)$ can be found by requiring that the integral of $P_\infty(E,l)$ is unity.

A. Yielding modeled as an activated process

In the SGR model, the yield rate $\Gamma(E,l)$ was assigned a functional form similar to that of an activated process [7]. This was based on the idea that each element can be represented by a single particle moving on a free energy landscape, which remains confined within a well of depth E until random fluctuations allow it to cross over this barrier into a different well, with a new barrier E'. Thus yielding can be identified with barrier crossing. This description is similar to that of activated processes in thermodynamic systems; however, the random fluctuations here are *not necessarily* due to the true thermodynamic temperature. They may arise rather from a form of homogeneous mechanical noise generated by nonlinear couplings between the elements; see Ref. [7] for a

fuller discussion on this point. To avoid possible confusion, this effective temperature is denoted by the symbol x rather than T.

Although the energy barrier of an element is initially E, as it becomes strained it will gain an elastic energy of $(1/2)kl^2$ and thus will have a smaller effective energy barrier $\Delta E = E - (1/2)kl^2$. Thus the yield rate will take the form

$$\Gamma(E,l) = \Gamma_0 \exp\left[-\frac{E - \frac{1}{2}kl^2}{x} \right], \qquad (5)$$

where the attempt rate Γ_0 sets the time scale of the yielding. The effective temperature x is constant in the SGR model, and essentially acts as a parameter of the model. However, since x may be generated in part by internal couplings between the elements, it should be allowed to vary with the state of the system, i.e., $x = x(\{P(E,l,t)\})$.

In this paper, we shall not consider the most general possible form for x, but shall instead focus on a more restricted class for which $x = x(\sigma, l)$. This corresponds to the realization that, as an element is strained, it may become more or less susceptible to the noise, and hence its "temperature" x may change. Allowing x to also depend on σ reflects that this change in susceptibility to noise may in part be a *global* phenomenon, i.e., the x of a given element may depend on the state of all of the elements around it. Clearly, deriving the actual $x(\sigma, l)$ for any given material would be a highly complicated task, of comparable difficulty to the original coarse-graining procedure described above.

For further simplicity, we shall not consider $x = x(\sigma, l)$ but shall instead focus on two limiting cases: $x = x(\sigma)$ is described in Sec. IV, and $x = x(l)$ is assumed in Sec. V and Sec. VI. The relevant results for the SGR model, which corresponds to the case of $x = (\text{const})$, are also summarized in Sec. III.

B. Natural units and the $\rho(E)$ distribution

We have yet to specify $\rho(E)$, the distribution of energy barriers E for elements that have just yielded. In the SGR model, $\rho(E)$ is assumed to have an exponential tail, $\rho(E) \sim e^{-E/E_0}$ as $E \to \infty$, which gives rise to a finite yield stress and diverging viscosity for some values of x, but not others [7]. Although it is possible to justify the occurrence of an exponential tail in some contexts [22], we prefer instead to treat this choice of $\rho(E)$, combined with the Arrhenius form of $\Gamma(E,l)$ (5), as a recipe for generating a yield stress within this simple picture of activated yielding. This may seem *ad hoc*, but it should be realized that jamming is in reality a many body effect, involving collective behavior between a large number of degrees of freedom. It should, therefore, come as no surprise that assumptions are required to describe jamming within this single-particle picture.

For much of this paper, we shall assume that $\rho(E)$ has an exponential tail, just as in the SGR model. In fact, for the numerics the definite form $\rho(E) = (1/E_0)e^{-E/E_0}$ has been used, although it is not expected that the precise shape of $\rho(E)$ for small E will alter the long time or steady state

behavior of the system. This is because small values of E correspond to elements with short expected lifetimes. Furthermore, it turns out that the oscillatory motion described in Sec. V does *not* depend on the choice of $\rho(E)$, and in Sec. VI the simpler form $\rho(E) = \delta(E - E_1)$ is used, with qualitatively similar results.

There remain three constants in the problem. These are the elastic constant k, the attempt rate Γ_0 in Eq. (5), and the constant E_0 in the definition of $\rho(E)$ given above. However, these can all be scaled out of the model. For instance, k sets the scale of the stress, and, therefore, can be removed by rescaling σ to σ/k. Similarly, Γ_0 gives the only intrinsic time scale in the system, and can be scaled out through t and $\dot{\gamma}$. Finally, E_0 sets the scale of the energy barriers, and can be scaled out through $x(\sigma, l)$.

In what follows, we have adopted *natural* units in which $k = \Gamma_0 = E_0 = 1$. This means that the actual values for t, γ, and σ given below should not be compared to experimental values without first rescaling with the appropriate k, E_0, and Γ_0 for the material in question. For example, the typical yield strain according to the $\Gamma(E, l)$ given in Eq. (5) is $\sqrt{2E_0/k}$, which is when the effective energy barrier vanishes. In natural units, this is of $O(1)$; however, for soft materials it will typically be of only a few percent, and will be even smaller for hard materials. Thus the scale of the local strains l, and, therefore, the scale of the global strain $\gamma(t)$, will generally be significantly smaller in real materials than with natural units.

III. SUMMARY OF THE STANDARD SGR MODEL

As discussed in the previous section, the standard SGR model is realized when (using natural units) the yield rate $\Gamma(E, l)$ is chosen to take an Arrhenius form with an energy barrier $E - (1/2)l^2$ and a constant effective temperature x, and $\rho(E)$ has an exponential tail $\rho(E) \sim e^{-E}$. Many results for this case are already known [6–8]. The purpose of this section is to briefly describe those results that will be referred to in later sections.

Let us assume that the system is driven by a given strain $\gamma(t)$, and that $\gamma(t) \sim \dot{\gamma} t$ as $t \to \infty$, where $\dot{\gamma} \neq 0$. Without loss of generality we take $\dot{\gamma} > 0$ hereafter. Under these conditions, the system will reach the steady state solution $P_\infty(E, l)$ already given in Eq. (4). The asymptotic stress σ is found by averaging the local strain l over $P_\infty(E, l)$, i.e., $\sigma = \langle l \rangle$, which defines the flow curve $\sigma(\dot{\gamma})$. Example flow curves for different values of x are shown in Fig. 1. In all cases the gradient $d\sigma/d\dot{\gamma}$ decreases with increasing $\dot{\gamma}$, indicating that the apparent viscosity $\eta \equiv \sigma/\dot{\gamma}$ decreases with $\dot{\gamma}$ and that the system is everywhere shear thinning.

It should also be noted that there is a a one-to-one correspondence between $\dot{\gamma}$ and σ. This means that every point on the curve can be reached in one of two ways: either by applying a known strain $\gamma(t) \sim \dot{\gamma} t$, as described above, or by imposing a constant stress σ. The uniqueness of the steady state solution ensures that the same $P_\infty(E, l)$ will be reached in both cases. Of course, this assumes that the steady state is
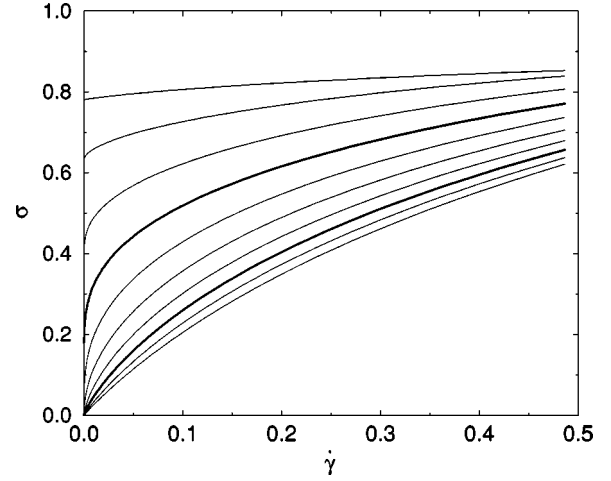

FIG. 1. Flow curves for a system with a constant x, i.e., the SGR model. From top to bottom, each line corresponds to a value of x increasing from 0.25 to 2.5 in steps of 0.25. The lines $x = 1$ and $x = 2$ have been highlighted. A finite yield stress $\sigma_Y \equiv \lim_{\dot{\gamma} \to 0}(\sigma)$ exists only for $x < 1$. The prior distribution is $\rho(E) = e^{-E}$.

reached at all, for which it must both exist and be stable. For the standard SGR model, the steady state solution is stable as long as it exists [7,8], but this does not hold for all $x(\sigma, l)$ under an imposed stress, as will be discussed in later sections.

The behavior of σ as $\dot{\gamma} \to 0^+$ depends upon the choice of x [7]. For instance, for $x > 2$ the stress scales as $\sigma \sim \dot{\gamma}$ and the system is Newtonian, whereas there is a power law fluid regime $\sigma \sim \dot{\gamma}^{x-1}$ for $1 < x < 2$. However, the most important regime for our purposes is $x < 1$, for which σ approaches a finite value. The yield stress σ_Y, defined by

$$\sigma_Y = \lim_{\dot{\gamma} \to 0^+} \sigma(\dot{\gamma}), \tag{6}$$

smoothly tends to zero as $x \to 1^-$ and remains zero for all $x \geq 1$. If a system with $x < 1$ has a stress $\sigma < \sigma_Y$ applied to it, then it will never reach a steady state with a finite $\dot{\gamma}$, simply because $P_\infty(E, l)$ for these parameters does not exist. Instead the strain will logarithmically creep according to $\gamma(t) \sim \ln t$ [8]. There may be a crossover to a different behavior at late times if σ is close to σ_Y, but it must always be true that $\dot{\gamma} \to 0^+$.

The logarithmic creep in $\gamma(t)$ under an imposed stress $\sigma < \sigma_Y$ is an important result. If it is realized in an experimental situation, then when the strain rate $\dot{\gamma} \sim 1/t$ drops below the resolution of the apparatus, which it must do at long times, it might be erroneously deduced that the system has stopped flowing altogether, i.e., $\dot{\gamma} \approx 0$. This is in accord with our intuitive notions about jamming: the sample initially flows when pushed, but later stops flowing, or "jams." One might argue that, technically, a jammed system should have $\dot{\gamma} = 0$ exactly, but it is not possible for any model in this class to sustain a finite stress without a finite $\dot{\gamma}$ (unless the sample is allowed to age for an arbitrarily long period of time before

being sheared; see Ref. [8]). This is because each individual element has a finite relaxation time until it yields and releases its stress, which can only be balanced by an increasing strain.

With this insight, we now *define* a "jammed" state for this class of systems to be a configuration that has a finite limiting stress σ_Y when it is driven by an arbitrarily small strain rate $\dot{\gamma}=0^+$. For the SGR model, this corresponds to $x<1$; however, for $x=x(\sigma)$ it may also depend on the history of the sample, as will now be discussed.

IV. JAMMING MODEL A: $x=x(\sigma)$

It is useful to recall the physical picture that underlies an $x=x(\sigma)$. As the system becomes sheared, either by an imposed strain γ or an imposed stress σ, it will become distorted, and this may affect its susceptibility to noise. The precise manner in which this happens will depend on the microscopic composition of the material in question. For the systems we are interested in, i.e., those that can shear thicken or jam, the distorted configuration is *less* susceptible to noise that the undistorted one. One way to incorporate this effect is to regard the system as becoming "colder" as its shear stress increases, which corresponds to a decreasing $x(\sigma)$. Thus setting $x=x(\sigma)$ provides a mechanism for allowing the effective temperature x to evolve with the global state of the system.

In this section we shall consider $x(\sigma)$ that takes values greater than 1 for some ranges of σ, and less than 1 for others. According to the results of the previous section, this should allow the system to change from a jammed to a flowing state in response to the driving, or more precisely, in response to changes in $\sigma(t)$. Thus we may be able to observe a shear-induced jamming transition (something that is not possible in the SGR model, for which the existence of a yield stress depends purely on the choice of the external parameter x). For clarity, we shall restrict our attention to the simplest choice of $x(\sigma)$ that has the potential to shear thicken and jam, namely, $x(\sigma)>1$ for small σ and $x(\sigma)<1$ for large σ, with a monotonic (possibly discontinuous) behavior for intermediate σ.

A. Steady state behavior

Although allowing x to vary in time according to $x=x[\sigma(t)]$ can complicate the transient behavior of the system, as described below, the steady state is easy to analyze. This is because the very definition of a steady state means that σ asymptotically approaches a constant value, and thus x also becomes constant. There is, therefore a straightforward procedure for generating the $x=x(\sigma)$ flow curves from those of constant x: for any given value of σ, one simply finds the SGR flow curve for the corresponding value of $x(\sigma)$ and reads off the required value of $\dot{\gamma}$. This amounts to interpolating between the various SGR flow curves. Some examples are given in Fig. 2 for various $x(\sigma)$ that change from 1.5 for small σ to 0.5 for large σ.

If $x(\sigma)$ takes values greater than 1 for small σ, but smaller than 1 for larger σ, then it may jam under an applied stress. However, for this situation to be realized, the applied stress must be simultaneously large enough that $x(\sigma)<1$, and also small enough that $\sigma<\sigma_Y$. Since the yield stress σ_Y also depends on x, the precise criterion for the upper yield stress to be attainable is that there is a range of σ for which

$$\sigma<\sigma_Y[x(\sigma)]. \tag{7}$$

This corresponds to the region in which the $x(\sigma)$ curve falls below the $\sigma_Y(x)$ curve when they are both plotted on the same axes, as in Fig. 3. For example, of the flow curves already presented in Fig. 2, only the third example obeys the criterion (7) for a finite range of σ. Imposing a stress σ from within this range will result in a system that is jammed in the sense that the strain logarithmically creeps, $\gamma(t)\sim\ln t$ and $\dot{\gamma}(t\to\infty)=0$.

Two additional complications arise when the system is driven by an imposed strain rate $\dot{\gamma}$ rather than an imposed stress. First, if $\dot{\gamma}$ is increased at a sufficiently slow rate that the system is always arbitrarily close to its steady state, the stress may undergo a discontinuous jump from one branch of the flow curve to another, as marked in Figs. 2(b) and 2(c). If $\dot{\gamma}$ is decreased in a similar fashion, then $\sigma(t)$ will follow the upper branch until it again jumps discontinuously at a *different* value of $\dot{\gamma}$. Thus the system exhibits *hysteresis*. Hysteresis due to nonmonotonic flow curves has also been observed experimentally [15–17,19]. The complementary form of nonmonotonicity, which would allow a discontinuous jump in $\dot{\gamma}$ for a small change in σ, cannot be realized in this class of models. This is because there is only one value of $x(\sigma)$, and hence one steady state solution, for any given value of σ.

The second complication concerns the stability of the jammed state. In Fig. 3, the yield stress $\sigma_Y(x)$ and an $x(\sigma)$ that obeys Eq. (7) for a range of σ have been plotted on the same axes. Also plotted is the line of σ that can be reached for a small but finite $\dot{\gamma}>0$, which converges to $\sigma_Y(x)$ as $\dot{\gamma}\to0$. These are the σ that can be realized in practice, since the steady state solution (4) is not defined for $\dot{\gamma}\equiv0$. For this example there are three roots: a "flowing" root with $\sigma=0^+$, and two "jammed" roots with finite $\sigma_Y>0$. The arrows in this diagram point in the direction in which the stress will be varying for a given point on the line $x(\sigma)$. This direction is based on the assumption that, for time scales over which x can be treated as a constant, which will certainly include the asymptotic regime, the system will behave like the SGR model and σ will evolve towards σ_Y. It is clear from this that all points tend to flow away from the middle root, which is, therefore, unstable. If the system is initially placed near to this root, it will undergo a transient and converge to either the higher root, or to the "flowing root" with $\sigma=0^+$.

Figure 3 can also be used to predict the stability of the steady state for finite $\dot{\gamma}$. As $\dot{\gamma}$ increases, the asymptotic stress $\sigma(\dot{\gamma})$ for the SGR model will move away from the yield stress curve, but will always remain a monotonic decreasing function of $\dot{\gamma}$ [7]. Thus a smoothly decreasing $x(\sigma)$ will only intersect with it one or three times; when there are three
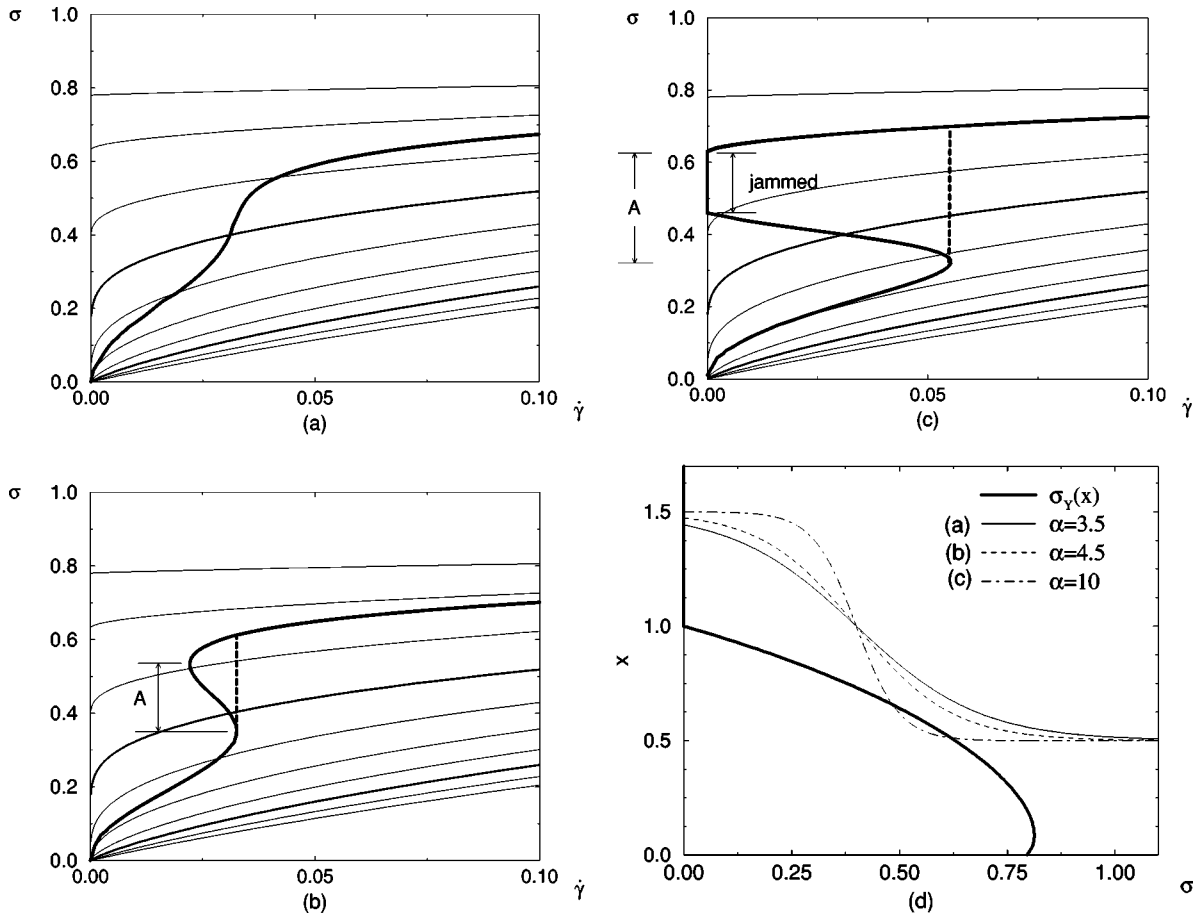
FIG. 2. Flow curves for $x(\sigma) = 1 - 0.5\tanh[\alpha(\sigma - 0.4)]$ (thick lines), where $\alpha = 3.5$ (a), 4.5 (b) and 10 (c). For comparison, the thin lines are the constant x curves from Fig. 1. In (b) and (c), the vertical dashed line represents the discontinuous jump in stress for a slowly increasing $\dot{\gamma}$, and the region marked "A" denotes the range of σ that is unstable under an imposed $\dot{\gamma}$, but is stable under an imposed σ. In (c), the range of σ for which the system is "jammed," i.e., $\sigma(0^+) > 0$, has also been marked. The $x(\sigma)$ for different α are plotted in (d), where it can clearly be seen that only for the $\alpha = 10$ case does $x(\sigma)$ drop below the yield stress curve.

roots, the middle one is always unstable, for precisely the same reasons as given in the previous paragraph. The range of σ that are unstable and cannot be realized under an imposed $\dot{\gamma}$ have been labeled "A" in Figs. 2(b) and (c). Note that the unstable roots correspond to regions of the flow curve with a negative gradient, as in experiments and from other theoretical considerations [13–18]. There are no stability issues for an imposed σ, for which there is always a single, stable root.

B. Transient behavior under an imposed $\dot{\gamma}$

There are in principle no difficulties in extending the results described above to a system that is driven by a time-dependent imposed stress $\sigma(t)$. As long as $\sigma(t)$ tends to a constant value σ_0 at long times, then the same steady state behavior as previously discussed will apply, with σ replaced by σ_0. The transient behavior does not affect the final state. However, this is not the case when the system is instead driven by an imposed strain rate $\dot{\gamma}(t)$. In this case, $\sigma(t)$ can vary in a manner that is difficult to predict in advance, so that

the final stress reached, and hence whether or not the system is jammed, will in general depend on the entire history of the system.

A concrete example of the history dependence of a yield stress is given in Fig. 4. Here, the system is first subjected to a step shear of magnitude γ_0, and is then continuously sheared at a rate $\dot{\gamma}$, i.e., $\gamma(t) = \gamma_0 + \dot{\gamma}t$. As $\dot{\gamma}$ tends to zero, the stress approaches an asymptotic value σ_Y; however, whether or not σ_Y is finite depends on γ_0. For $\gamma_0 = 1$ the stress is seen to be converging to a finite value $\sigma \approx 0.65$, but for $\gamma_0 = 0.1$ it rather tends to a "flowing" state with $\sigma = 0^+$ (more precisely, $\sigma \propto \dot{\gamma}^{0.5}$ as $\dot{\gamma} \to 0^+$). The system can be said to exhibit strong long-term memory, where the use of the word "strong" means that the memory of an earlier perturbation of finite duration does not decay to zero with time [8,23–25].

The choice of $x(\sigma)$ used in the previous example is in fact the same as that plotted in the stability diagram, Fig. 3. This allows for a striking illustration of the instability of the middle root that lies near the point $\sigma \approx 0.3$ on the stability diagram. Plotted in Fig. 5 are the $\sigma(t)$ curves for a fixed $\dot{\gamma}$
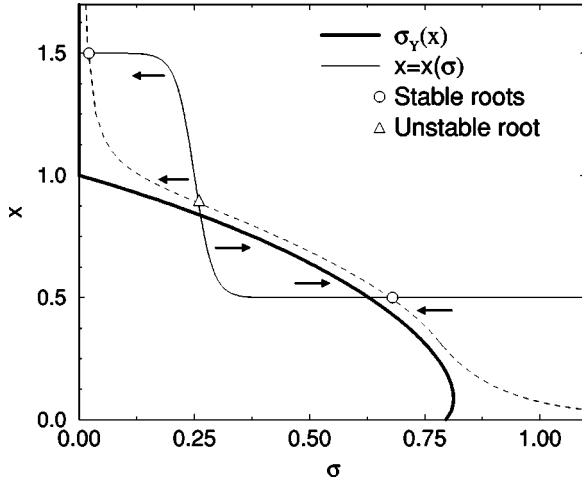
FIG. 3. Plot of the yield stress $\sigma_Y(x)$ from the SGR model, overlayed with a particular choice of $x(\sigma)$ that changes value from 1.5 to 0.5 with increasing stress (the actual functional form is $x(\sigma) = 1 - \frac{1}{2} \tanh[25(\sigma - 0.25)]$). The dashed line is a schematic representation of the asymptotic stress $\sigma(t \to \infty)$ for a small but finite $\dot{\gamma}$, which is what is actually attainable for these models. The arrows represent the direction in which the stress will vary for a constant x, and explain the given stability of the roots.

$= 10^{-3}$ and a range of values $0.1 \leqslant \gamma_0 \leqslant 1$. It is clear that the stress will always diverge away from the unstable root at late times, no matter how finely γ_0 is tuned. Thus only the roots at $\sigma = 0^+$ and $\sigma \approx 0.65$ are stable, as previously claimed.

There are many other complications that can arise due transient behavior in a strain-controlled system. For instance, all of the $\sigma(t)$ curves plotted in Fig. 4 reach their global minimum $\sigma_{\min}$ at a time $1 \ll t \ll 1/\dot{\gamma}$. It can be shown that
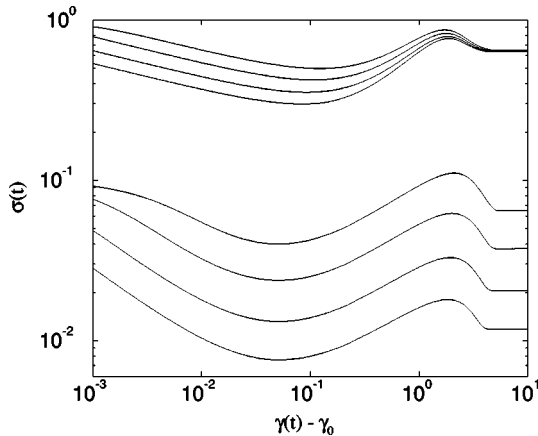

FIG. 4. Plot of stress versus strain for $\gamma(t) = \gamma_0 + \dot{\gamma} t$ and the same $x(\sigma)$ as in Fig. 3. The upper set of lines corresponds to $\gamma_0 = 1$ and the lower set to $\gamma_0 = 0.1$. Within each set, the lines refer to (from top to bottom) $\dot{\gamma} = 3 \times 10^{-3}$, 10^{-3}, 3×10^{-4}, and 10^{-4}. As $\dot{\gamma} \to 0^+$, the upper curves are seen to be converging to $\sigma \to \sigma_Y \approx 0.65$, whereas the lower curves are approaching a zero-stress state according to $\sigma \approx k \dot{\gamma}^{0.5}$, where k is an arbitrary constant. In all cases the system was first allowed to reach equilibrium under zero shear before the step shear γ_0 was applied.
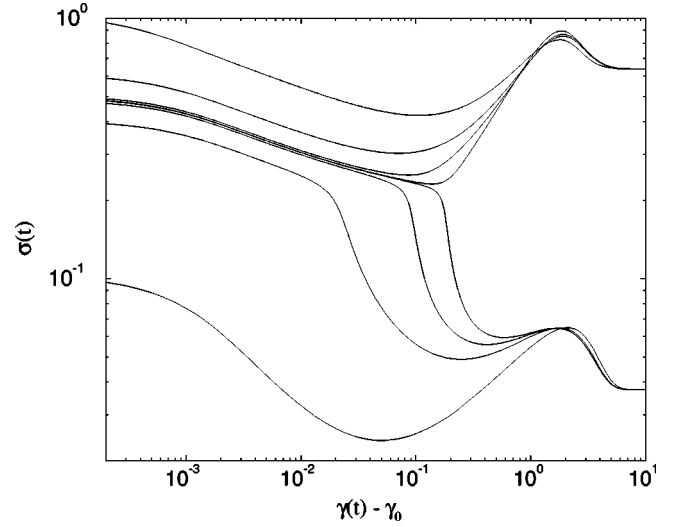

FIG. 5. The variation in stress for the system of Fig. 4 driven by the imposed strain $\gamma(t) = \gamma_0 + \dot{\gamma} t$ with $\dot{\gamma} = 10^{-3}$, demonstrating the inability to reach the root at $\sigma \approx 0.3$. From bottom to top on the left-hand side, the "initial condition" γ_0 takes the values $\gamma_0 = 0.1$, 0.4, 0.48, 0.49, 0.491, 0.5, 0.6, and 1.

$\sigma_{\min}$ becomes arbitrarily small as $\dot{\gamma} \to 0^+$. Since this corresponds to a state with a high effective temperature $x(\sigma_{\min} = 0^+) > 1$ in which the stress is rapidly dissipated, then if $\dot{\gamma}$ is sufficiently small, $\sigma(t)$ will remain low and the system will crossover to the flowing root, irrespective of γ_0. However, this effect can be reversed if the initial step shear is replaced by a smoothly varying $\dot{\gamma}(t)$, such as one that exponentially decays towards its final value of $\dot{\gamma}$, which is more like what could be attained in an actual rheometer. We will not pursue these complications any further here.

In summary, the SGR model generalized to allow the effective temperature x to vary with the global stress σ can exhibit, for suitable choices of $x(\sigma)$: *hysteresis* in $\sigma(t)$ for slowly varying $\dot{\gamma}$, as seen from the flow curves in Fig. 2; shear induced *jamming*, as in Fig. 4; and *strong history dependence* of the existence of a yield stress.

V. JAMMING MODEL B: $x = x(l)$

The second limiting form for $x = x(\sigma, l)$ to be considered is one that depends only on the local strain, $x = x(l)$. This marks a more drastic departure from the SGR model than the $x(\sigma)$ considered in the previous section, since now every element will generally have a different effective temperature x. The steady state will, therefore, be different from that of the SGR model, and it will not now be possible to map the flow curves for $x(l)$ across from those for constant x. One could also envisage regions of the parameter space for which the steady state cannot even be reached. Indeed, this is precisely what we find: for some finite region of parameter space, the system reaches an oscillatory regime under an imposed stress, but not under an imposed strain. This is the central finding of this section.

The physical justification in choosing $x = x(l)$ is similar to that already discussed for $x = x(\sigma)$, i.e., it is assumed that the
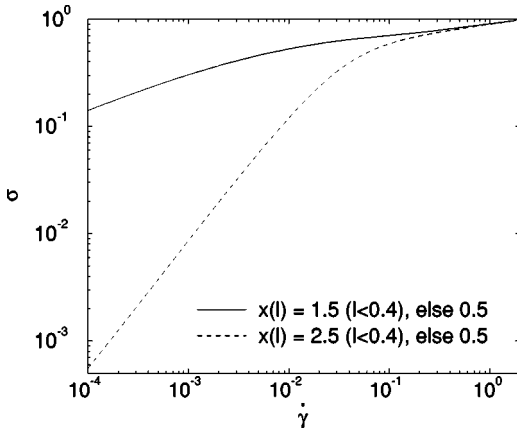
FIG. 6. Examples of typical flow curves when x depends on the local strain l. Here, $x(l)=0.5$ for $l>0.4$, but takes the higher value of 1.5 (solid line) or 2.5 (dashed line) for $l<0.4$. These lines were generated from the steady state solution of the master equation.

FIG. 7. The strain $\gamma(t)$ under an imposed stress $\sigma_0=0.05$ for a system in which x depends on the local strain according to $x(l) = 1.8$ for $l<0.4$ and $x(l)=0.8$ for $l>0.4$. (Inset) The strain rate $\dot{\gamma}(t)$ for the same data after the transient.

material can become more or less susceptible to noise in its strained state. The main difference is that this is now assumed to be a local effect, that can be described purely on the level of individual elements. Just as in the previous section, we shall focus our attention on $x(l)$ that decrease with l, since it is these that have the potential to exhibit shear thickening.

A. Monotonicity of the flow curves

Given $x(l)$, the steady state stress σ for a given $\dot{\gamma}$ can be found by calculating the mean strain $\langle l \rangle$ for the steady state solution (4). Some example flow curves are plotted in Fig. 6. They are clearly monotonic: their gradient is everywhere positive, and there is a one-to-one relationship between σ and $\dot{\gamma}$. In these figures, the $x(l)$ were chosen to vary in a stepwise manner, taking a value $x>1$ for $l<0.4$ and a lower value $x<1$ for $l>0.4$. This is typical of the $x(l)$ employed in this section. However, the monotonicity result is entirely general and applies for any $x=x(l)$, as demonstrated in Appendix B.

The physical reason for the monotonicity of the flow curves is that the elements are uncoupled when $x=x(l)$ and the system is driven by an imposed strain $\gamma(t)$. That is, the expected strain reached before a given element yields does not depend on the state of any other elements. This is *not* true for the general case $x=x(\sigma,l)$, when the value of x for an element depends on the global stress σ, and thus on the state of the rest of the system. As long as independence holds, the average strain reached before each individual element yields, and hence the global stress σ, can only increase with increasing $\dot{\gamma}$. Thus the flow curves must be monotonic.

The monotonicity of the flow curves is an important finding. As mentioned in Sec. I, rheological instabilities often arise when the system has been driven to a point on its flow curve that has a negative gradient. Fluctuations can then cause spatial inhomogeneities to arise, such as shear bands with either the same stress and different strain rates, or equal strain rates but differing stresses [13,14]. Alternatively, tem-
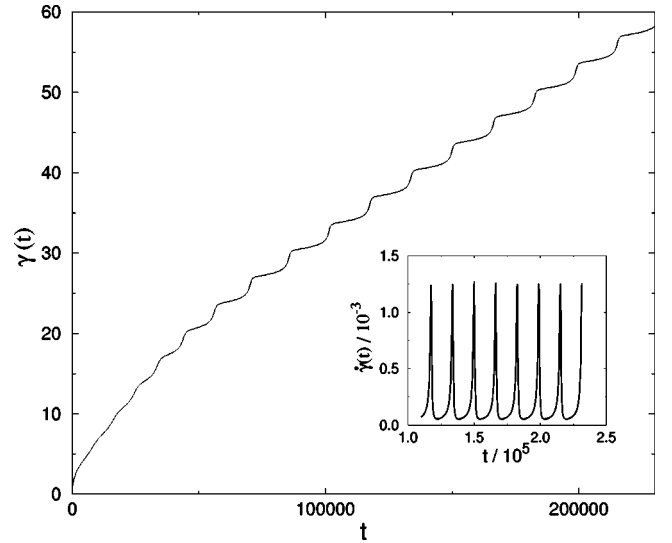
poral oscillations may be observed [17,18]. Since the flow curves for $x=x(l)$ have no regions of negative slope, one would not expect any instabilities to appear in this model. Nonetheless temporal oscillations in $\dot{\gamma}$ do occur for a finite range of imposed σ, as we now describe.

B. Oscillatory behavior under an imposed σ

The monotonicity result described above was attributed to the independence of the elements, which is only true for a strain controlled system. By contrast, the elements become coupled under an imposed σ since, for example, a single element yielding causes the mean strain to decrease slightly, which must be immediately countered by an increase in $\dot{\gamma}$, *which affects every element in the system*. Thus collective behavior can now occur. In fact, this collective behavior cannot alter any system that has already reached steady flow, which we know is identical for strain and stress controlled systems. Thus as long as the stress-controlled system reaches steady flow, it will fall onto the same monotonic flow curve as before. However, the couplings between the elements can drastically alter the transient behavior, to such an extent that steady flow may never be reached.

An example of collective behavior is given in Fig. 7, which shows $\dot{\gamma}(t)$ for a system driven by an imposed stress $\sigma=0.05$. As before, this plot was generated by numerically integrating the master equation (1) from an initially unstrained state, using the procedure described in Appendix A. For this example, the system undergoes a short transient before entering into an oscillatory regime, in which $\dot{\gamma}(t)$ varies with a single period of oscillation. There is no suggestion of a decay in the amplitude of the oscillation in $\dot{\gamma}(t)$ over the largest simulation times attainable, even when plotted against $\ln t$ (not shown), suggesting that this is the true asymptotic behavior. For different choices of $x(l)$ it is not possible to
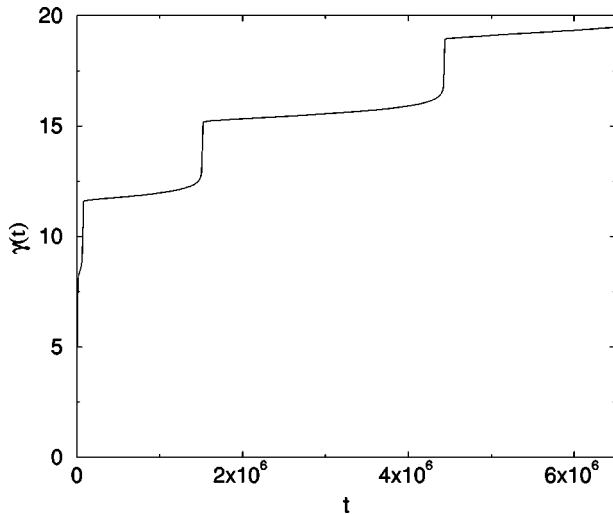
FIG. 8. The strain $\gamma(t)$ under an imposed stress $\sigma_0 = 0.1$ for $x(l) = 1.5$ for $l < 0.7$, 0.5 for $l > 0.7$. Despite the long times attained, there is no clear indication of a single period of oscillation.

identify a single period of oscillation, as demonstrated in Fig. 8. It is not yet clear if this behavior represents a distinct regime with more than one period of oscillation, possibly even a precursor to chaotic behavior, or if it is merely a long-lived transient that eventually crosses over to either steady flow or a single-period oscillation at later times.

The extensive simulation times means that we have so far been unable to map out the class of $x(l)$ that give rise to an oscillatory or otherwise nonsteady state. Nonetheless we can make the following observation. For all of the oscillatory cases that we have observed thus far, $x(l)$ changes from a value in the range $1 < x < 2$ for small l, to a value $x < 1$ for larger l. Other choices of $x(l)$ may produce an oscillatory transient, but its amplitude always seems to decay to zero in time. It is not clear to us why only this class of $x(l)$ can produce a stable oscillatory regime, but it is tempting to note that the requirement that $1 < x < 2$ for small l is also the range of x for which the SGR model does not have a linear regime under an imposed σ [8]. That is, a significant proportion of elements will eventually gain a finite strain, no matter how small σ is, and thus the variation in $x(l)$ will eventually be "felt."

Once a suitable $x(l)$ has been found, it is possible to move in and out of the nonsteady regime by varying the applied stress σ. Generally, we find that a high σ gives rise to steady flow, and low σ produces oscillations; however, the excessive simulation times needed for small σ means that we have not been able to rule out another crossover to steady flow as $\sigma \rightarrow 0^+$. Within the oscillatory regime, the mean strain rate averaged over a period of oscillation is generally much lower than that predicted by the flow curve. For the examples already given, the mean strain rate deviates from the flow curve by a factor of 2 for the oscillations shown in Fig. 7, and by two orders of magnitude for the (possibly transient) oscillations of Fig. 8. Again, we have been unable to fully characterize this behavior with the available simulation resources. To an extent, these problems will be alleviated by considering a simplified model considered in Sec.

VI. Before turning to consider this, we provide a qualitative description of the oscillatory behavior in terms of the local strains l.

C. Qualitative description of the evolution of the system in the oscillatory phase

The mechanism behind the oscillatory behavior can be qualitatively understood by inspecting the evolution of the $P(E, l, t)$ distribution during a single period of oscillation. As an example, a suitable sequence of snapshots is given in Fig. 9. To aid in the interpretation of these figures, it is useful to recall some properties of the master equation (1). First, the convective term $\dot{\gamma} \partial P / \partial l$ means that any maxima or minima in $P(E, l, t)$ will move in the direction of increasing l at a rate $\dot{\gamma}(t)$. These extrema will eventually disappear when large values of l are reached, and the yield rate $\Gamma(E, l)$ becomes very high. Also, there is a flux of newly yielded elements at $l = 0$, which have barriers E weighted according to $\rho(E)$.

Since the oscillatory behavior is by definition cyclical, it is somewhat arbitrary where one chooses to start the sequence of snapshots. In Fig. 9 we have chosen times corresponding to before, during, and just after the point when $\dot{\gamma}$ reaches its maximum value. In the first snapshot, $P(E, l, t)$ is concentrated into two regions: a sharp peak at $l \approx 0$, and a broader peak with l in the range $1 < l < 3$. The first peak is 'hot' in the sense that it has the higher value of $x(l)$, but since it has a low strain, it does not significantly contribute to the total stress σ. The second peak, although highly strained, lies in a region in which $x(l)$ is small, and, therefore, has a low rate of yielding. As long as the yield rate is low, so too is the rate of stress loss from elements that belong to this peak. Therefore, the strain rate $\dot{\gamma}$ will also be low, and indeed this first example corresponds to a system in which $\dot{\gamma}$ is close to its minimum value.

This state of affairs is not stable, however. Although the yield rate of the highly strained elements is low, it is nonetheless nonzero, and, therefore, so is $\dot{\gamma}$. Consequently the whole system is being convected at a finite rate, so the elements in the high-l region are becoming more strained. This *decreases* their effective energy barrier $\Delta E = E - (1/2)l^2$, which *increases* their yield rate. But an increased yield rate means an increased $\dot{\gamma}$, which in turn increases the rate at which the elements are becoming more strained, which increases their yield rate yet more, and so on. This description is that of a *positive feedback loop*, which causes $\dot{\gamma}$ to increase at ever faster rates until all of the heavily strained elements have been depleted. The second snapshot in Fig. 9 show the state of the system shortly before this has happened.

At the same time that the highly strained elements are being depleted, $\dot{\gamma}$ is close to its maximum value and consequently $P(E, l, t)$ in the small l region becomes somewhat flat, certainly much flatter than under a small $\dot{\gamma}$. This can clearly be seen in the second and third snapshots of Fig. 9. When $\dot{\gamma}$ again falls to lower values, this flat part of the dis-
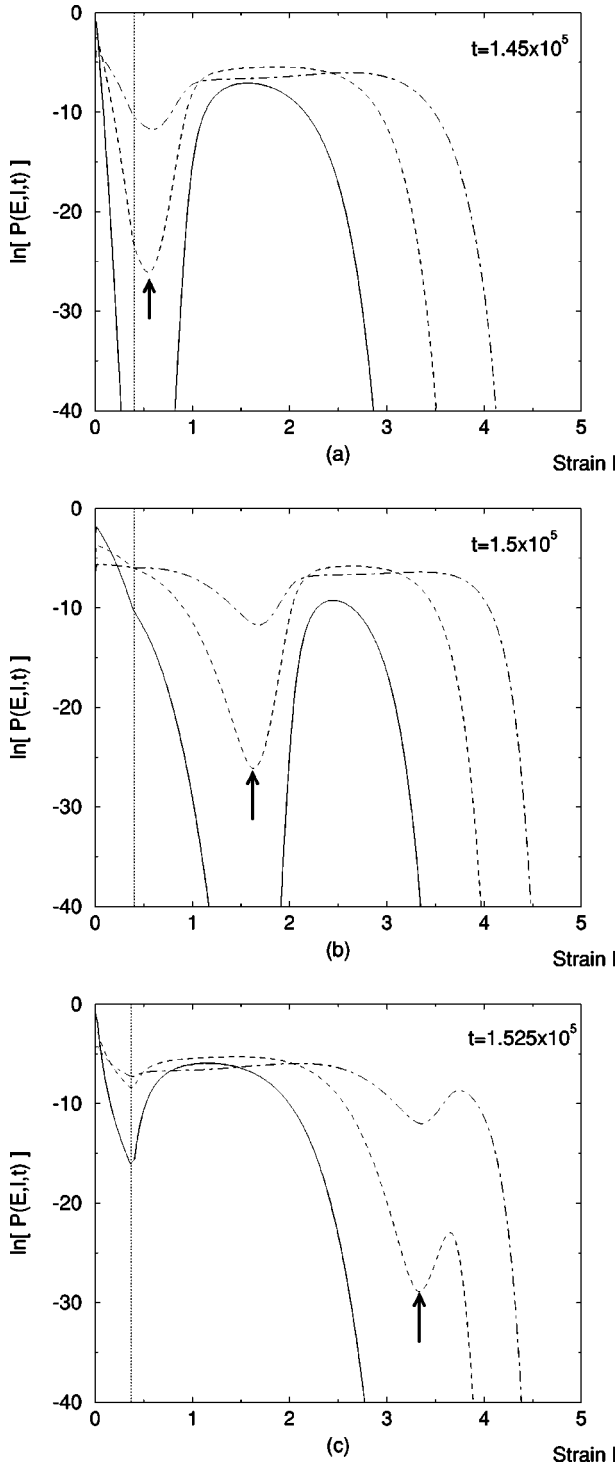
FIG. 9. Snapshots of $P(E,l,t)$ for the same system as in Fig. 7 at three different times. For clarity only three values of E are shown, namely, $E=8$ (solid line), $E=10$ (dashed line), and $E=12$ (dot-dashed line). The chosen times correspond to just before (a), during (b), and just after (c) the point at which $\dot{\gamma}$ reaches it maximum value. The period of the oscillation is approximately $\Delta t = 1.6\times10^4$, so that the time between (a) and (c) comprises roughly $\frac{1}{2}$ of a single oscillation. In each case, the l at which $x(l)$ changes from 1.8 to 0.8 is represented by a vertical dotted line, and the arrow points to the *same* dip in the $E=10$ distribution, which moves to the right under the action of $\dot{\gamma}$.

tribution will start to decay as the elements within it yield. However, the yield rate depends on $x(l)$, and since $x(l)$ changes to a lower value at $l=0.4$, $P(E,l,t)$ will decay much more rapidly for l just smaller than 0.4 than for l just greater than 0.4. Thus a dip will occur around the point $l \approx 0.4$, which can clearly be seen in the final snapshot. As time increases, this dip will become more pronounced until the system can again be separated into a population of highly strained elements and a second population with $l\approx0$. This is where we began, and thus the cycle is complete.

VI. JAMMING MODEL C: $x=x(l)$, MONODISPERSE E

It is possible to more completely describe the oscillatory regime for a simplified version of the model where every element has the same energy barrier E_1. This formally corresponds to a "monodisperse" prior distribution $\rho(E) = \delta(E-E_1)$, as opposed to the exponential $\rho(E)=e^{-E}$ which has been employed in all of the earlier sections. The reduction in the number of degrees of freedom that this entails significantly decreases the simulation times, and, therefore, allows for a more thorough numerical investigation of the model. It is also possible to derive an analytical criterion for the stability of the steady state, as described below.

Furthermore, the very fact that a monodisperse system also has an oscillatory regime clearly demonstrates that this phenomenon is robust. In particular, it does not require the usual SGR assumption of an exponential tail to $\rho(E)$. Therefore, the possible existence of a yield stress, which was so central to the history-dependent jamming scenario at controlled $\dot{\gamma}$ described in Sec. IV, is not necessary. This robustness means that the mechanism behind the oscillations at controlled σ may be realizable in a much broader range of models than the restricted set considered here and, possibly, may also occur in real materials.

The emergence of oscillations in this monodisperse model has been separately discussed elsewhere [20]. Here we supply extra details, such as the stability analysis of the steady flow state. For the sake of completeness, the overall behavior of the model will also be briefly described, although we refer the reader to Ref. [20] for a fuller discussion of many of the points raised below.

A. Steady state behavior for monodisperse E

Perhaps the most immediate consequence of only allowing a single barrier E_1 is that the system can never have a finite yield stress. Indeed, in the linear regime $\dot{\gamma}\rightarrow0^+$, the steady state stress is just $\sigma\sim\dot{\gamma}e^{E_1/x(0)}$, which vanishes with $\dot{\gamma}$. There are no qualitative differences for $x<1$, $1<x<2$, etc., as in the SGR model. The complete lack of a yield stress means that a monodisperse system with $x=x(\sigma)$ will *not* exhibit a jamming transition, in contrast to the situation for a $\rho(E)$ with an exponential tail described Sec. IV.

One respect in which the monodisperse E model is similar to the exponential $\rho(E)$ case is that its flow curves for $x =x(l)$ are also monotonic. In fact, the monotonicity proof given in Appendix B holds for arbitrary $x(l)$ and $\rho(E)$. Thus there are no regions on the flow curve with a negative slope,
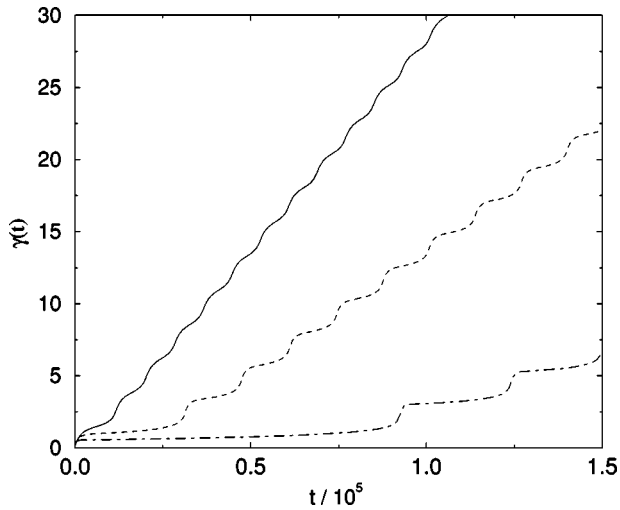
FIG. 10. The strain $\gamma(t)$ for a monodisperse system with E_1 $=5$ under an imposed step stress $\sigma=0.1$ (solid line), 0.13 (dashed line) and 0.2 (dot-dashed line) at a time $t=0$, demonstrating a decrease in the mean $\dot{\gamma}$ with σ. Here, $x(l)=1$ for $l<0.4$ and $x=0.4$ for $l>0.4$. The system was initially unstrained.
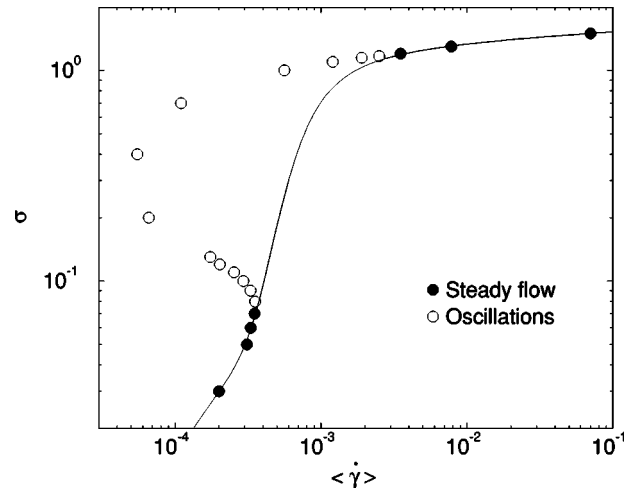

FIG. 11. The flow curve for the same system as in Fig. 10 under an imposed stress. The circles are the $\dot{\gamma}$ as measured from the simulations, either in the steady state (solid circles) or in the oscillatory regime (open circles). In the latter cases, $\dot{\gamma}$ was averaged over a whole number of oscillations. The sizes of the circles are larger than the error bars. For comparison, the theoretical flow curve for the steady state solution $P_\infty(E,l)$ is plotted as a solid line.

and, therefore, there are no ranges of control parameters for which one might normally expect bulk shear banding to arise. Just as in the previous section, however, oscillatory behavior can be realized under an imposed constant stress.

B. The oscillatory regime

As in the polydisperse case, the monodisperse model exhibits an oscillatory regime under conditions of imposed stress, but not under an imposed $\dot{\gamma}$. However, the oscillatory regime in the monodisperse model differs from the polydisperse case in that only single-period oscillations have so far been observed. There is no suggestion of the more complex nonsteady behavior hinted at earlier in Fig. 8, for example. Some examples of the oscillatory behavior in the monodisperse case are given in Fig. 10. Here, the strain $\gamma(t)$ is shown for three systems with $E_1=5$ and the same $x(l)$, but different imposed σ. Remarkably, the mean strain rate $\langle\dot{\gamma}\rangle$, where the use of the angular brackets now denotes $\dot{\gamma}$ averaged over a single period of oscillation, is clearly a *decreasing* function of σ, in complete contrast to the monotonic flow curve.

Varying σ over a wider range of values reveals that steady flow is reached for either sufficiently small or sufficiently large imposed stresses; only for intermediate σ are oscillations observed. The $\langle\dot{\gamma}\rangle$ as read off from the simulations are plotted against σ in Fig. 11, overlaid with the steady state flow curve. It is clear that, if the system reaches a steady state, it falls onto the flow curve and, therefore, the dependence of $\langle\dot{\gamma}\rangle$ with σ is monotonic. Within the oscillatory regime, however, the $\langle\dot{\gamma}\rangle$ line deviates from the flow curve to an extent that it even becomes nonmonotonic for a broad range of σ.

The shape of the oscillations varies with σ. Close to either transition to the steady flow regime, the oscillations are ap-

proximately sinusoidal, indicating that there is only a single, finite frequency of oscillation at the transition, the amplitude of which vanishes with the onset of steady flow. Further into the oscillatory regime, $\dot{\gamma}$ can no longer be decomposed into a single harmonic, but instead approaches a wave form in which most of the variation in $\dot{\gamma}$ is compressed into a small fraction of the total period of oscillation. Consequently $\gamma(t)$ approaches an almost rectangular, staircase shape. The mechanism underlying the rapid increase in $\dot{\gamma}$ is the same positive feedback loop that has already been discussed for the polydisperse case, as can be seen by inspecting the evolution of the $P(l)$ distribution with time [20].

Near to the transition points at $\sigma=\sigma_c$, the amplitude of the oscillation appears to vanish as $|\sigma-\sigma_c|^\alpha$ with $\alpha>0$, as demonstrated in Fig. 12. Data fitting suggests that the lower threshold lies at $\sigma_c\approx0.07$ with a value of $\alpha\approx0.7$, and that the upper threshold is at $\sigma_c\approx1.204$ and has a different value of $\alpha\approx0.2$. However, the range of values given in this figure is somewhat limited, constituting only an order of magnitude of variation in $|\sigma-\sigma_c|$ and an even narrower range of amplitudes. The reasons for this are purely technical: close to the transition points, the amplitude decays very slowly in time to its asymptotic value, rendering the required simulation times impractically long. Hence it is conceivable that the true values of α are significantly different from those found here. In particular, a value of $\alpha=0.5$ for both cases, as expected for a Hopf bifurcation [26], cannot be ruled out.

Finally, plotted in Fig. 13 is the product of the mean strain rate $\langle\dot{\gamma}\rangle$ and the period of oscillation T for different values of σ. To first order, $\langle\dot{\gamma}\rangle T$ is seen to be independent of σ, which suggests that the oscillatory regime can be characterized by a single strain $l^*\sim\langle\dot{\gamma}\rangle T$. In this case $l^*\approx2.3$, which is also the typical increase in γ during a single cycle of oscillation. A
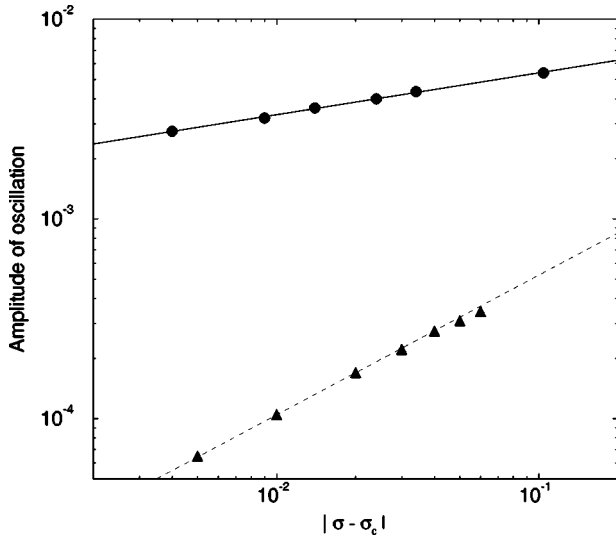
FIG. 12. The amplitude of the oscillation, defined as $\frac{1}{2}|\dot{\gamma}_{\max} - \dot{\gamma}_{\min}|$, against the distance from the transition between the steady and oscillatory regimes. The upper data set (circles) corresponds to the transition at $\sigma_c = 1.204$, and the lower set (triangles) corresponds to $\sigma_c = 0.07$. For comparison, the solid straight line has a slope of 0.21, and the dashed line has a slope of 0.7.

possible interpretation of l^* is that it is the amount by which the system needs to be strained until the positive feedback loop discussed earlier starts to dominate the system behavior, causing it to "reset" to the start of its cycle. If this is correct, then l^* should correspond to the point at which highly strained elements have the same yield rate as unstrained elements, i.e., $\Gamma(0) \approx \Gamma(l^*)$. Rough calculations based on this assumption give $l^* \approx \sqrt{2E_1[1 - x(\infty)/x(0)]}$, which for this example predicts $l^* \approx 2.4$, in fair agreement with the observed value.
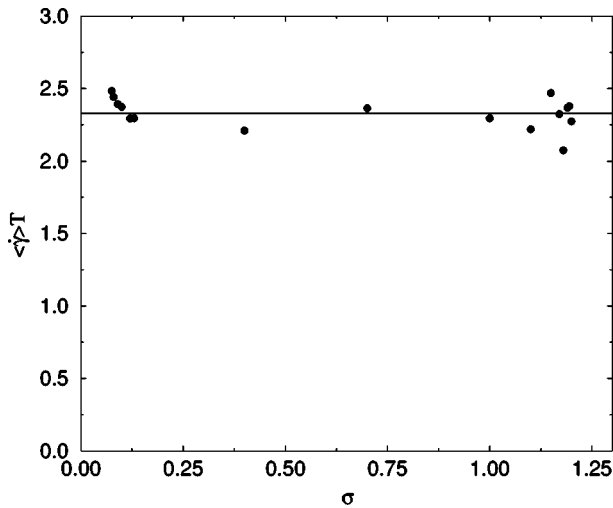

FIG. 13. The product of the mean strain rate $\langle \dot{\gamma} \rangle$ and the period of oscillation T for different stresses σ, demonstrating that this quantity is approximately constant. The solid horizontal line represents $\langle \dot{\gamma} \rangle T = 2.33$.

C. Analysis of the stability of the steady state

A second advantage of the monodisperse model is that it is possible to derive an analytical criterion for the stability of the steady state at fixed driving shear stress σ, although even in this simplified case the resulting expression is still somewhat unwieldy. Suppose steady flow is reached with a strain rate $\dot{\gamma}_\infty = \dot{\gamma}_\infty(\sigma)$. Then the corresponding $P_\infty(l)$ is

$$P_\infty(l) = \mathcal{N} \exp\left[-\frac{1}{\dot{\gamma}_\infty} \int_0^l \Gamma(l') dl' \right], \tag{8}$$

where the normalization constant $\mathcal{N}$ is fixed by the constraint $\int_0^\infty P_\infty(l) dl = 1$. We now look for eigenfunctions $\{p(l), g\}$ and eigenvalues $\{s\}$ of the linearized relaxation operator by writing

$$P(l,t) = P_\infty(l) + \varepsilon p(l) e^{st}, \tag{9}$$

$$\dot{\gamma}(t) = \dot{\gamma}_\infty + \varepsilon g e^{st}. \tag{10}$$

In these expressions, g is a real constant, and the real functions $p(l)$ remain to be found. The complex constant s determines the stability of the steady state: it is unstable precisely when $\mathrm{Re}(s) > 0$, since the amplitude of the perturbation will then increase exponentially in time. Conversely, it is stable when $\mathrm{Re}(s) < 0$. The frequency of the oscillatory part of the motion near to the steady state is $\mathrm{Im}(s)/2\pi$ [26].

The unknown function $p(l)$ can be found by inserting Eqs. (9) and (10) into the master equation and neglecting terms of $O(\varepsilon^2)$, which gives

$$p'(l)\dot{\gamma}_\infty + p(l)[s + \Gamma(l)] = -g P_\infty'(l) \tag{11}$$

$$= \frac{g\Gamma(l)}{\dot{\gamma}_\infty} P_\infty(l). \tag{12}$$

This is just a first-order differential equation in l and integrates to

$$p(l) = \frac{g\mathcal{N}}{\dot{\gamma}_\infty^2}\left[A + \int_0^l dl' \Gamma(l') e^{sl'/\dot{\gamma}_\infty} \right]$$

$$\times \exp\left[-\int_0^l dl' \frac{s + \Gamma(l')}{\dot{\gamma}_\infty} \right]. \tag{13}$$

The constant A can be found by imposing $\int_0^\infty dl P(l,t) = 1$, i.e., $\int_0^\infty dl p(l) = 0$.

Also, since we are considering a stress-controlled system, $\sigma = \langle l \rangle$ must remain constant and hence

$$\int_0^\infty dl p(l) l = 0. \tag{14}$$

This global constraint allows the value of s to be specified. Inserting Eq. (13) into Eq. (14) gives, after some manipulations, the following equation for s:

$$\int_0^\infty dl_1 \int_0^\infty dl_2 (l_2 - l_1) P_\infty(l_1) P_\infty(l_2) e^{-s(l_1+l_2)/\dot{\gamma}_\infty}$$

$$\times \int_0^{l_2} dl \Gamma(l) e^{sl/\dot{\gamma}_\infty} = 0. \qquad (15)$$

Although this equation cannot be rearranged to give an expression for s in terms of the system parameters, as would be desired, it is still enough to show that a purely exponential variation away from the steady flow cannot be observed. This follows from the observation that the first line in Eq. (15) is an odd function in $l_2 - l_1$, but the second line is a strictly increasing function of l_2 when $\mathrm{Im}(s) = 0$. Hence the equation cannot be obeyed for a purely real s, and the transient behavior close to the steady state must include an oscillatory component, which is consistent with the simulation results.

VII. DISCUSSION

One of the most striking findings of this work has been the observation of oscillations in $\dot{\gamma}(t)$ under a constant imposed stress σ for some $x = x(l)$, as described in Sec. V and Sec. VI. Some consequences of this phenomenon have already been discussed in Ref. [20]. Two further points will be discussed here: the identification of the dominant physical mechanisms, and the relationship to so-called "stick-slip" behavior observed in other systems. Both of these will be considered in turn.

A. Physical picture and analogous phenomena

In Sec. V C, the mechanism behind the oscillatory behavior was explained in terms of two separated populations of elements: a "cold" population of highly strained elements with a low x, and a "hot" population of elements with $l \approx 0$ and a high x. It was explained how the cold elements can give rise to a positive feedback loop, causing $\dot{\gamma}(t)$ to rapidly increase until the cold elements have yielded. At the same time, a new population of cold elements is produced from the hot one.

Known instances of rheological instability are often explained in terms of the spatial coexistence of subpopulations, or phases. For instance, the temporal oscillations in viscosity observed in wormlike micelles under an imposed stress was attributed to a slowly fluctuating interface between a fluid phase and shear-induced structures [18]. For surfactant solutions in the lyotropic lamellar phase, it was attributed to coexisting ordered and disordered phases [17]. However, these instabilities occur in the vicinity of nonmonotonic regions of the flow curve. Spatial instabilities, such as shear banding, can also be found near to where the flow curve has a negative gradient [13]. By contrast, the temporal oscillations observed in our models arise even though they are by assumption spatially homogeneous, and the flow curves are everywhere monotonic.

This suggests that the mechanism behind the oscillatory behavior seen here has not yet been observed in a rheological context. It is, therefore, sensible to look further afield for

analogous phenomena. One possibility comes from mathematical biology. The Glass-Mackey equation describes the variation in time of the size of a population of white blood cells in response to a hormonal control system [27]. It has a form similar to that of a first-order differential equation, but includes a feedback term that depends on the state variable at an earlier time. This *delay* corresponds to the maturation time of white blood cells from stem cells. Because of this delay, the population size can vary in time in a nontrivial manner, including oscillatory behavior and chaos [27].

That some form of time delay may also play a role within our $x(l)$ model is clear: once an element becomes "cold," its yield rate remains very low until some time later, when it becomes sufficiently strained that its yield rate becomes comparable to that of "hot" elements. Thus there is a delay between when an element first becomes cold and when it yields, although here the delay time is not constant but depends on $\gamma(t)$. Thus it is possible that the oscillatory behavior observed for $x = x(l)$ could be described by a simplified equation, similar in form to the Glass-Mackey equation. This is a particularly enticing proposition, as the Glass-Mackey equation is capable of producing chaos, and chaotic behavior has also been observed in surfactant solutions [28,29], albeit in the signature of $\sigma(t)$ under an imposed $\dot{\gamma}$. It is not yet clear to us if a meaningful mapping between the two models is possible.

B. Oscillatory behavior or "stick-slip?"

Deep into the oscillatory regime, the wave form of $\dot{\gamma}(t)$ throughout a single period of oscillation becomes increasingly "sharp," with most of the variation in $\dot{\gamma}(t)$ occurring in just a small fraction of the total period of oscillation. The ratio of the maximum value of $\dot{\gamma}(t)$ to its minimum has been shown to exceed two orders of magnitude, and we see no reason to deny that greater separations may be attained for different parameter values.

It is tempting to refer to this behavior of $\dot{\gamma}(t)$ as "stick-slip" behavior, in which the system is "stuck" until the short duration of time in which $\dot{\gamma}$ rapidly accelerates to its maximum value, corresponding to a "slip" event. This kind of response is also observed in earthquakes [9], ultrathin liquid films [10], and granular media [11,12], for example. However, we have instead chosen to refer to the variation in $\dot{\gamma}(t)$ as merely "oscillatory," since the underlying physics seems to be somewhat different to the examples of stick-slip behavior mentioned above. In particular, the term stick slip is usually employed to refer to a surface friction phenomenon, whereas the models studied in this paper have no surface, or indeed any form of spatial definition. They are only intended to describe the bulk behavior of a material. Furthermore, we only find oscillations in $\dot{\gamma}(t)$ under an imposed σ, and never *vice versa*, whereas stick slip seems to more usually (although not exclusively) refer to variations in the (normal) stress under a constant driving velocity. Thus to avoid possible confusion, we choose not to refer to the behavior observed in the models as stick slip.

VIII. SUMMARY

We have introduced a range of schematic models that are capable of exhibiting a form of jamming under an imposed stress σ. The models are based on the SGR model of Sollich *et al.*, but differ in that the effective temperature x is no longer constant, and can instead vary with the state of the system through either the global stress σ or the local strain l. We have considered choices of x that decrease for increasing σ or l, which is relevant to the study of shear thickening materials. These models have no spatial definition, and thus by construction cannot exhibit any form of spatial heterogeneity.

For $x = x(\sigma)$, the flow curves can be extracted from the known curves for constant x. Many choices of $x(\sigma)$ produce flow curves with nonmonotonic regions, which exhibit hysteresis in $\sigma(t)$ under ramping the strain rate $\dot{\gamma}(t)$ first upwards and then downwards. Furthermore, a subset of these $x(\sigma)$ also give rise to a *jammed* state for a range of applied stresses, in that the strain $\gamma(t)$ creeps logarithmically, $\gamma(t) \propto \ln(t)$. The criterion for this to arise is that the curve of $x(\sigma)$ drops below the SGR yield stress curve $\sigma_Y(x)$ when they are plotted on the same axes. For an imposed strain rate that decays to zero at late times, a jammed configuration was defined as one with a finite asymptotic stress, $\sigma(t) \sim \sigma_Y > 0$ as $\dot{\gamma}(t) \rightarrow 0^+$ and $t \rightarrow \infty$. It was found that whether or not a jammed configuration was reached depends on the entire strain history of the system, a situation that was referred to as *history-dependent jamming*.

For $x = x(l)$, the flow curves are always monotonic, and steady flow is always reached under a constant imposed strain rate $\gamma(t) \sim \dot{\gamma}t$. However, for a range of imposed stresses and some choices of $x(l)$, steady flow is not realized. Numerical integration of the master equation demonstrated that $\dot{\gamma}(t)$ oscillated around a well-defined mean with a single period of oscillation. The possibility of more complex non-steady behavior in some regions of parameter space could not be ruled out. A similar oscillatory behavior occurs with a simpler model in which every element has the same energy barrier [20], which suggests that this phenomenon is robust. Finally, we discussed the relationship between this oscillatory behavior and that observed in experiments, and considered analogous phenomena from fields outside of rheology.

APPENDIX A: SIMULATION DETAILS

Direct numerical integration of the master equation (1) has proven to be unstable with respect to discretization errors. Instead, the results in this paper were generated from the transformed equation

$$\frac{\partial P(E, \Delta l, t)}{\partial t} = -\Gamma(\Delta l + \gamma(t)) P(E, \Delta l, t) + \omega(t)$$

$$\times \delta(\Delta l + \gamma(t)) \rho(E), \qquad (A1)$$

where $\Delta l = l - \gamma(t)$. This removes the convective term and dramatically improves numerical stability. The discrete probability distribution $P_{ij} = P(i \delta E, j \delta l)$ was defined on a rectangular mesh of points $\{ij\}$ and evolved according to Eq. (A1) by using a straightforward Euler method. A further refinement was to average both the evolution equation (A1) and the initial conditions over the ranges $(E, E + \delta E)$ and $(\Delta l, \Delta l + \delta l)$. This significantly reduces the number of mesh points required for the simulations to properly converge, without unduly increasing the algorithmic complexity. The delta function was treated as a triangle of base width $2 \delta l$ and height $1/\delta l$, but any sufficiently narrow function gave the same results.

Two classes of initial conditions were employed, but the long-time behavior of the system was found to be identical in both cases. Only the short-term behavior varied, and then only in a nonessential manner. For the sake of completeness, the initial conditions were: (i) A "quench" $P_0(E, l) = \delta(l) e^{-E}$, which corresponds to the unstrained equilibrium at $x = \infty$, or (ii) $P_0(E, l) = \delta(l)(1/E_0) e^{-E/E_0}$ with $E_0 = [1 - 1/x(l = 0, \sigma = 0)]^{-1}$, which corresponds to an unstrained system that has been allowed to reached equilibrium. Note that this second initial state is only defined for $x(l = 0, \sigma = 0) > 1$ [30].

The strain $\gamma(t)$ is only known *a priori* for a strain-controlled system. When it is rather a known stress $\sigma(t)$ that is applied, $\gamma(t)$ must be chosen at every time step so that the actual stress does not differ from $\sigma(t)$ by more than a tolerance parameter $\varepsilon \ll 1$. To ensure that this condition was satisfied in our simulations, a series of trial strain rates $\dot{\gamma}^{(1)}, \dot{\gamma}^{(2)}, \dot{\gamma}^{(3)} \dots$ were generated and tested on a replica mesh P_{ij}^*. The P_{ij} were not updated until a suitable $\dot{\gamma}$ had been found.

The trial values $\dot{\gamma}^{(i)}$ were generated as follows. For a continuous time variable, $\dot{\gamma}(t) = \langle l \Gamma(l) \rangle_{P(t)} + \dot{\sigma}(t)$ exactly, as seen by multiplying the master equation (1) by l and integrating over all E and l. This is, therefore, the sensible choice for $\dot{\gamma}^{(1)}$. However, integrating over a finite time step δt inevitably introduces errors of $O(\delta t)$, and so the integrated stress will differ from the required value by some small amount $\delta\sigma$. Reintegrating with $\dot{\gamma}^{(2)} = \dot{\gamma}^{(1)} - \delta\sigma$ will, therefore, reduce the error to a smaller amount $O(\delta t^2)$. This procedure can be repeated to generate a series of successively better estimates $\dot{\gamma}^{(3)}$, $\dot{\gamma}^{(4)}$, etc. For our choice of $\varepsilon = 10^{-6}$, we have found that typically 3–5 such trials are needed at every time step.

APPENDIX B: MONOTONICITY OF THE FLOW CURVES

The purpose of this appendix is to show that the flow curves are monotonic for any yield rate $\Gamma(l)$ that depends only on the local strain l. This includes the thermally acti-

vated $\Gamma(l)$ with $x=x(l)$, possibly constant, but not when x also depends on the stress σ. It also applies for an arbitrary prior barrier distribution $\rho(E)$.

The steady state solution $P_\infty(E,l)$ has already been given in Eq. (4). The asymptotic yield rate $\omega_\infty \equiv \lim_{t\to\infty}\omega(t)$ is fixed by ensuring that this expression normalizes to unity,

$$\omega_\infty^{-1} = \frac{1}{\dot{\gamma}}\int dE \int dl \rho(E) e^{-f(\sigma,l)/\dot{\gamma}}, \tag{B1}$$

where we have introduced the shorthand notation $f(\sigma,l)=\int_0^l \Gamma(\sigma,l')dl'$. The stress is $\sigma=\langle l\rangle_\infty$, where the angular brackets '$\langle\rangle_\infty$' denote the average over $P_\infty(E,l)$. If Γ depends on σ, then a σ must be chosen that is consistent with Eq. (4). In general there can be more than one suitable σ.

First consider the case $\Gamma=\Gamma(l)$, so $f=f(l)$. Then by differentiating $\langle l\rangle_\infty$ and using Eq. (4),

$$\frac{\partial\sigma}{\partial\dot{\gamma}}=\frac{\sigma}{\omega_\infty}\frac{\partial\omega_\infty}{\partial\dot{\gamma}}-\frac{\sigma}{\dot{\gamma}}+\frac{1}{\dot{\gamma}^2}\langle lf(l)\rangle_\infty. \tag{B2}$$

Similarly, the ω_∞ equation (B1) can be differentiated to give

$$\frac{1}{\omega_\infty}\frac{\partial\omega_\infty}{\partial\dot{\gamma}}=\frac{1}{\dot{\gamma}}-\frac{1}{\dot{\gamma}^2}\langle f(l)\rangle_\infty. \tag{B3}$$

Combining these two expressions produces

$$\dot{\gamma}^2\frac{\partial\sigma}{\partial\dot{\gamma}}=\langle lf(l)\rangle_\infty-\sigma\langle f(l)\rangle_\infty \tag{B4}$$

$$=\langle(l-\sigma)f(l)\rangle_\infty \tag{B5}$$

$$=\langle(l-\sigma)[f(l)-f(\sigma)]\rangle_\infty. \tag{B6}$$

The final line in this equation is valid as $f(\sigma)$ is a constant, so $\langle(l-\sigma)f(\sigma)\rangle_\infty=f(\sigma)\langle l-\sigma\rangle_\infty=0$. Since $f(l)$ is an increasing function of l, the quantity in the angular brackets in (B6) is positive both for $l<\sigma$ and for $l>\sigma$, and vanishes smoothly at $l=\sigma$. Thus the left-hand side must be positive, i.e., σ always increases with $\dot{\gamma}$, as claimed.

The same conclusion does not hold when $\Gamma=\Gamma(\sigma,l)$. Since σ depends on $\dot{\gamma}$, differentiating the steady state solution now gives rise to an extra term on the right-hand side of (B2),

$$\frac{\partial\sigma}{\partial\dot{\gamma}}=\frac{\sigma}{\omega_\infty}\frac{\partial\omega_\infty}{\partial\dot{\gamma}}-\frac{\sigma}{\dot{\gamma}}+\frac{1}{\dot{\gamma}^2}\langle lf(\sigma,l)\rangle_\infty-\frac{1}{\dot{\gamma}}\langle lg(\sigma,l)\rangle_\infty\frac{\partial\sigma}{\partial\dot{\gamma}}. \tag{B7}$$

using $g(\sigma,l)=\int_0^l[\partial\Gamma(\sigma,l')/\partial\sigma]dl'$. Proceeding as before,

$$\dot{\gamma}^2\frac{\partial\sigma}{\partial\dot{\gamma}}=\frac{\langle(l-\sigma)f(\sigma,l)\rangle_\infty}{1+\frac{1}{\dot{\gamma}}\langle lg(\sigma,l)\rangle_\infty}. \tag{B8}$$

Thus it is now possible for the gradient to diverge if $\langle lg(\sigma,l)\rangle$ is sufficiently negative, i.e., if $\Gamma(\sigma,l)$ decreases sufficiently rapidly with σ. For the particular case of $\Gamma(\sigma,l)=\exp[-(E-\frac{1}{2}l^2)/x(\sigma)]$, the gradient of the flow curve diverges at any point such that

$$x'(\sigma)=\frac{-x^2(\sigma)\dot{\gamma}}{\left\langle l\int_0^l\left(E-\frac{1}{2}l'^2\right)\exp[-(E-\frac{1}{2}l'^2)/x]dl'\right\rangle_\infty}. \tag{B9}$$

We can see no obvious physical interpretation of this mathematical criterion.

---

[1] M. D. Ediger, C. A. Angell, and S. R. Nagel, J. Phys. C **100**, 13 200 (1996).

[2] S. F. Edwards and D. V. Grinev, in *Jamming and Rheology*, edited by A. J. Liu and S. R. Nagel (Taylor and Francis, New York, 2001); also e-print cond-mat/9905114.

[3] A. J. Liu and S. R. Nagel, Nature (London) **396**, 21 (1998).

[4] V. Trappe, V. Prasad, L. Cipelletti, P. N. Segre, and D. A. Weitz, Nature (London) **411**, 772 (2001).

[5] M. E. Cates, J. P. Wittmer, J.-P. Bouchaud, and P. Claudin, Phys. Rev. Lett. **81**, 1841 (1998).

[6] P. Sollich, F. Lequeux, P. Hébraud, and M. E. Cates, Phys. Rev. Lett. **78**, 2020 (1997).

[7] P. Sollich, Phys. Rev. E **58**, 738 (1998).

[8] S. M. Fielding, P. Sollich, and M. E. Cates, J. Rheol. **44**, 323 (2000).

[9] C. H. Holz, Nature (London) **391**, 37 (1998).

[10] I. S. Aranson, L. S. Tsimring, and V. M. Vinokur, e-print cond-mat/0101186.

[11] M. Lubert and A. de Ryck, Phys. Rev. E **63**, 021 502 (2001).

[12] I. Albert, P. Tegzes, R. Albert, J. G. Sample, A.-L. Barabási, T. Vicsek, and P. Schiffer, Phys. Rev. E **64**, 031307 (2001); e-print cond-mat/0102523.

[13] P. D. Olmsted, Curr. Opin. Colloid Interface Sci. **4**, 95 (1999).

[14] C.-Y. D. Lu, P. D. Olmsted, and R. C. Ball, Phys. Rev. Lett. **84**, 642 (2000).

[15] O. Volkova, S. Cutillas, and G. Bossis, Phys. Rev. Lett. **82**, 233 (1999).

[16] D. Bonn, J. Meunier, O. Greffier, A. Al-Kahwaji, and H. Kellay, Phys. Rev. E **58**, 2115 (1998).

[17] A. S. Wunenburger, A. Colin, J. Leng, A. Arnéodo, and D. Roux, Phys. Rev. Lett. **86**, 1374 (2001).

[18] Y. T. Hu, P. Boltenhagen, and D. J. Pine, J. Rheol. **42**, 1185 (1998).

[19] H. M. Laun, J. Non-Newtonian Fluid Mech. **54**, 87 (1994).

[20] D. A. Head, A. Ajdari, and M. E. Cates, Europhys. Lett. (to be published).

[21] F. Lequeux and A. Ajdari, Phys. Rev. E **63**, 030 502 (2001).

[22] J.-P. Bouchaud and M. M'ezard, J. Phys. A **30**, 7997 (1997).

[23] J.-P. Bouchaud, L. F. Cugliandolo, J. Kurchan, and M. M'ezard, in *Spin Glasses and Random Fields* (World Scientific, Singapore, 1998).

[24] L. F. Cugliandolo and J. Kurchan, Phys. Rev. Lett. **71**, 173 (1993).

[25] L. F. Cugliandolo and J. Kurchan, Philos. Mag. **71**, 501 (1995).

[26] P. Glendinning, *Stability, Instability, and Chaos: An Introduction to the Theory of Nonlinear Differential Equations* (Cambridge University Press, Cambridge, 1994).

[27] L. Glass and M.C. Mackey, *From Clocks to Chaos* (Princeton University Press, Princeton, 1988).

[28] R. Bandyopadhyay, G. Basappa, and A. K. Sood, Phys. Rev. Lett. **84**, 2022 (2000).

[29] R. Bandyopadhyay and A. K. Sood, Europhys. Lett. **56**, 447 (2001).

[30] C. Monthus and J.-P. Bouchaud, J. Phys. A **29**, 3847 (1996).